International Journal of Greenhouse Gas Control 42 (2015) 525–533

Contents lists available at ScienceDirect

International Journal of Greenhouse Gas Control

journal homepage: www.elsevier.com/locate/ijggc

Experimental study of CO_2 convective dissolution: The effect of color indicators

C. Thomas[a,*], L. Lemaigre[a], A. Zalts[b], A. D'Onofrio[c], A. De Wit[a,*]

[a] Université libre de Bruxelles (ULB), Nonlinear Physical Chemistry Unit, Faculté des Sciences, CP231, 1050 Brussels, Belgium
[b] Instituto de Ciencias, Universidad Nacional General Sarmiento, Argentina
[c] Grupo de Medios Porosos, Universidad de Buenos Aires, Argentina

ARTICLE INFO

Article history:
Received 13 April 2015
Received in revised form 29 August 2015
Accepted 4 September 2015

Keywords:
Convective dissolution
Fingering
Reactive dissolution
CO_2 sequestration
Color indicator

ABSTRACT

Color indicators are often used for visualization purposes in experimental studies of CO_2 convective dissolution in aqueous solutions. We analyze and compare here experimentally the hydrodynamic fingering pattern induced by CO_2 dissolution in aqueous solutions of various color indicators. Characteristics of the convective patterns are measured as a function of time to study whether the choice of the color indicator or its concentration has an influence on the dynamics. We also compare the visualization of the fingering instability with a color indicator to the pattern observed with a Schlieren technique tracking changes in index of refraction. We find that color indicators are able only to track pH isocurves and do not always allow to capture the full extent of the fingers. We conclude that color indicators should be used with caution in experimental works devoted to quantify properties of CO_2 convective dissolution.

1. Introduction

Within the global context of climate change, carbon dioxide (CO_2) sequestration into deep saline aquifers is one of the technologies being considered in order to reduce the accumulation of anthropogenic CO_2 in the atmosphere (Metz et al., 2005; Firoozabadi and Cheng, 2010). Upon injection of supercritical CO_2 into these porous geological formations, the less dense CO_2 rises above the aqueous phase, spreads laterally under the upper impermeable cap rock and starts to dissolve into the underlying brine. This leads to a buoyantly unstable stratification of denser CO_2-enriched brine on top of less dense pure brine, which can give rise to buoyancy-driven convective fingering in the host fluid. This hydrodynamic instability is a favorable process for CO_2 sequestration as it accelerates the mixing of CO_2 into the aqueous phase and enhances the safety of the storage in the saline aquifer (Ennis-King and Paterson, 2005; Hassanzadeh et al., 2005, 2006; Riaz et al., 2006; Yang and Gu, 2006; Pau et al., 2010; Elenius and Johannsen, 2012). As these dynamics are difficult to analyze *in-situ*, a growing interest is developing for the experimental study of convective dissolution in aqueous solutions at laboratory scale.

Recently, controlled laboratory-scale experiments have analyzed CO_2 convective fingering in aqueous solutions with the use of small reactors or Hele-Shaw cells. This latter apparatus is made of two transparent glass or Plexiglas plates (typically a few tens of cm wide) separated by a narrow gap, generally less than 2 mm. CO_2 under subcritical (Okhotsimskii and Hozawa, 1998; Arendt et al., 2004; Song et al., 2005; Kneafsey and Pruess, 2010, 2011; Kilpatrick et al., 2011; Wylock et al., 2011, 2013, 2014; Faisal et al., 2013; Mojtaba et al., 2014; Thomas et al., 2014; Outeda et al., 2014; Kirk et al., 2014) or supercritical (Khosrokhavar et al., 2014) conditions is brought in contact with aqueous solutions, reactive or not, in the quasi two-dimensional space between the glass plates, in order to study the characteristics of the buoyancy-driven instability setting up in the aqueous solution upon CO_2 dissolution. Similar convective dissolution in partially miscible systems have been well characterized experimentally in other two-layer systems (Budroni et al., 2014). Chemical reactions have also been shown recently to be able to control such buoyancy-driven fingering (Budroni et al., 2014; Thomas et al., 2014).

Other experimental studies have focused on convective mixing developing at interfaces between either fully miscible (Neufeld et al., 2010; Backhaus et al., 2011; Tsai et al., 2013; Slim et al., 2013; MacMinn and Juanes, 2013) or immiscible (Cardoso and Andres, 2014) solvents. As shown theoretically (Hidalgo et al., 2012; Budroni et al., 2014; Thomas et al., 2014; Kim, 2014), the temporal evolution of density profiles in such miscible or immiscible systems

* Corresponding authors.
E-mail addresses: cathomas@ulb.ac.be (C. Thomas), adewit@ulb.ac.be (A. De Wit).

http://dx.doi.org/10.1016/j.ijggc.2015.09.002
1750-5836/

is different from those in partially miscible systems typical of the CO_2–water interface for which the evolution of the density stratification in the host phase is solubilization limited and not diffusion limited. As a consequence, the development and the characteristics of the convective dynamics taking place in miscible, immiscible or partially miscible systems will not be the same quantitatively. Nevertheless, interest of characterizing quantitatively convective processes in these various systems is growing and a precise measurement of the properties of the convective motions in the fluids is then needed.

The development of the convective dynamics in CO_2–water two-layer systems can be visualized with the help of an optical technique sensitive to changes in refractive index generated by density gradients such as a Schlieren technique (Okhotsimskii and Hozawa, 1998; Arendt et al., 2004; Thomas et al., 2014; Khosrokhavar et al., 2014) or interferometry (Wylock et al., 2011, 2013, 2014; Song et al., 2005). In some cases however, the presence of acidic dissolved CO_2 is detected with a color indicator sensitive to pH changes which allows to visualize the pattern with a simple camera thanks to a change in color of the fingers (Kneafsey and Pruess, 2010, 2011; Outeda et al., 2014; Kilpatrick et al., 2011; Faisal et al., 2013; Kirk et al., 2014; Mojtaba et al., 2014). There are some underlying hypotheses in the use of such color indicators for visualization purposes: the pattern revealed by the indicator is supposed to be exactly the same as the convective pattern developing upon CO_2 dissolution and the effect of indicators on the dynamics is assumed to be negligible. However, Outeda et al. (2014) have shown that the dispersion curves of the fingering instability induced by the dissolution of CO_2 in water are different if the concentration of color indicator contained in water was varied. Moreover, in the context of miscible acid-base fronts, studies of buoyancy-driven instabilities have shown that the patterns observed and the development of the dynamics strongly depend on the presence or not of a color indicator (Almarcha et al., 2010; Kuster et al., 2011). Nevertheless, most of the studies visualizing convective patterns with color indicators usually neglect these aspects and sometimes do not even mention the color indicator used or its concentration.

In this context, we study experimentally the impact of the use of color indicators on the visualization of convective dissolution of CO_2 in aqueous solutions. To do so, we analyze the development of CO_2 fingering in water containing increasing concentrations of bromocresol green or bromocresol purple. The length of the fingers and the relative area of the convective pattern (ratio of the area of the convective pattern to the total picture area) are measured as a function of time in order to determine whether the choice of the color indicator or its concentration has an influence on the pattern observed. The CO_2 convective dissolution is also studied in NaOH solutions containing different color indicators and the visualization of the convective dynamics by color changes of pH indicator is compared to the pattern observed with a Schlieren technique sensitive to gradients in index of refraction. We show that the shape and the characteristics of the pattern visualized strongly depend on the color indicator selected to perform the study. We also demonstrate that, if the color indicator is not chosen properly, some part of the convective dynamics may not be visualized, giving rise to an inaccurate quantitative characterization of the patterns. On the other hand, we find that the presence of a color indicator in the solution does not impact substantially the development of the convective dynamics in the experiments considered here.

2. Experimental system

The experiments are carried out in a Hele-Shaw cell, widely used in the study of CO_2 convective dissolution (Mojtaba et al., 2014; Kneafsey and Pruess, 2010, 2011; Slim et al., 2013; Tsai et al., 2013; Wylock et al., 2011, 2013, 2014; Thomas et al., 2014; Faisal et al., 2013; Backhaus et al., 2011; MacMinn and Juanes, 2013; Cardoso and Andres, 2014; Outeda et al., 2014; Kirk et al., 2014; Kilpatrick et al., 2011). In this confined environment, provided the gap width a between the plates is smaller than the characteristic wavelength of the pattern studied, the dynamics is analogous to that of a two-dimensional flow within a porous medium (Darcy's law), with a permeability κ governed by the separation between the plates ($\kappa = a^2/12$).

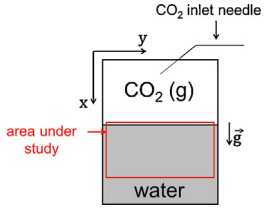

Fig. 1. Schematic representation of the system. The cell is partially filled with deionized water and gaseous CO_2 is introduced through the top of the cell using a narrow needle inserted between the glass plates.

Our Hele-Shaw cell is made of two 200 mm × 200 mm × 6 mm flat glass plates maintained together vertically in the gravity field and separated by a silicone-rubber spacer of thickness a = 1.0 mm. For each experiment, the cell is partially filled with deionized water containing a color indicator, and gaseous CO_2 is introduced through the top of the cell at a pressure of 1 atm and constant flow rate (6 L/h), using a narrow needle inserted trough the top of the cell between the glass plates (Fig. 1). The top of the cell is covered but not completely sealed in order to allow the excess of gaseous CO_2 to flow outside the cell and keep the gaseous phase inside the cell at atmospheric pressure. Note that "pure" water is used here instead of salted water in order to focus on the effect of the color indicator only.

The dynamics is observed under transmitted white light and a camera captures the dynamics at successive times (0.2 fps) during the experiment. Each experiment runs 30 min and is carried out at room temperature.

3. Visualization of the dynamics

When CO_2 dissolves in the aqueous solution, it reacts with water to form carbonic acid (H_2CO_3), which instantaneously dissociates into bicarbonate (HCO_3^-) and carbonate (CO_3^{2-}) ions, following the equilibrium equations:

$$CO_2(g) \leftrightharpoons CO_2(aq) \quad (1)$$

$$CO_2(aq) + H_2O \leftrightharpoons H^+ + HCO_3^- \quad (2)$$

$$HCO_3^- \leftrightharpoons H^+ + CO_3^{2-} \quad (3)$$

These equilibria in water will change several physical and chemical properties of the aqueous solution. Some of these changes can be detected with an adequate method to visualize the convective dynamics in the solution.

On one hand, the density of the solution increases due to the presence of dissolved CO_2, HCO_3^- and CO_3^{2-} (Blair and Quinn, 1968; Haynes, 2014). Density gradients set up vertically in the solution, giving rise to a buoyantly unstable stratification and eventually triggering the instability. These density gradients will generate gradients in refractive index exploited by optical visualization techniques, like Schlieren systems, to track the dynamics (Settles, 2001).

On the other hand, the release of H^+ during these equilibria lowers the pH of the aqueous solution. This decrease can be of several pH units, depending on the concentration of dissolved CO_2 in water. For our experimental conditions (gaseous CO_2 flowing

at atmospheric pressure above the interface), the pH decreases approximately to 4. The presence of dissolved CO_2 in water can therefore be detected with an appropriate pH indicator. Such indicators are large organic molecules that exhibit acid-base properties. Its acidic form (HInd) has a different color than the conjugated base (Ind^-). The general equilibrium of a pH indicator in water can be formulated as:

$$HInd \leftrightharpoons H^+ + Ind^- \quad (4)$$

The concentration of H^+ fixes thus which form of the indicator is dominant in the solution and hence what its color is. Upon dissolution of CO_2 in water and subsequent release of H^+ by (2) and (3), the equilibrium (4) is displaced to the left, changing the ratio between [HInd] and [Ind^-], and a change of color can be noticed in the solution. Generally, pH indicators change their color between the basic and the acid form when the pH of the solution is close to its pK_a, where K_a is the acid dissociation constant.

Among the best known pH indicators, only a few have a transition range corresponding to the pH decrease due to CO_2 dissolution in water. Bromocresol green (BG) has been largely used for visualization purposes in CO_2 experiments (Kneafsey and Pruess, 2010, 2011; Outeda et al., 2014; Faisal et al., 2013). Recently, a few experiments also considered bromocresol purple (BP) (Kilpatrick et al., 2011; Kirk et al., 2014), which has a transition range for larger pH than BG and should therefore be more sensitive to the dissolution of CO_2, but to the best of our knowledge, no complete study has been performed with this color indicator. In this context, we selected these two indicators to visualize the convective dissolution of CO_2 in water. Solutions are prepared with deionized water containing BG (sodium salt, $C_{21}H_{13}Br_4NaO_5S$, molar mass Mr = 720.00) and BP ($C_{21}H_{16}Br_2O_5S$, Mr = 540.22). They are characterized by slightly different transition ranges, between pH 5.4 and 3.8 (blue to yellow) for BG and between pH 6.8 and 5.2 (purple to yellow) for BP.

To investigate the impact of the presence of a color indicator in water on the development of the CO_2 convective instability, the dynamics is studied in solutions of BG at 3 different concentrations: 5.0×10^{-5} mol/L, analogous to the concentration of Kneafsey and Pruess (2010) and below which the color contrast between the acidic and basic forms of BG becomes too weak to be observed; 1.00×10^{-4} mol/L, comparable to the concentration of Outeda et al. (2014); and 1.000×10^{-3} mol/L, a high concentration near the solubility limit of BG, chosen in order to observe the behavior of the dynamics in a concentrated solution. The convective dynamics is also visualized under the same initial conditions in BP solutions of intermediate concentration (1.00×10^{-4} mol/L). A set of five experiments was done for each concentration. In most color indicator applications (titration for example), the concentration of indicator in solution is taken as low as possible provided the color of the solution is clearly observable. In some situations, the maximum concentration of indicator is still 10 times smaller than the concentration of other dissolved species. Following Henry's law at atmospheric pressure, the concentration of dissolved CO_2 at the interface is expected to be on the order of 10^{-2} mol/L. Even if it is impossible to know exactly the concentration field of the different dissolved species inside a finger, we can assume that the concentration of color indicator we use is sufficiently smaller than the concentration of dissolved CO_2, at least in the two lowest concentrations of indicator considered here.

4. Results and discussion

4.1. Qualitative results

Fig. 2 shows two stages of the development of the buoyancy-driven convective instability which develops upon dissolution of gaseous CO_2 in water containing BP and BG at different concentrations. When gaseous CO_2 starts to flow in the head-space of the cell, the color of the solution is uniform and the interface between the liquid and the gas is flat. After a few seconds, a thin yellow boundary layer appears just below the interface, indicating that the CO_2 starts to dissolve in water and to influence the color of the indicator. This diffusive layer becomes larger in time and is destabilized in a few minutes, giving birth to small yellow fingers of denser CO_2 sinking from the interface (Fig. 2(a)). Over time, CO_2 fingers grow, enlarge and penetrate deeper into the solution with some non-linear effects like merging (Fig. 2(b)).

First, we observe that the initial color of BG solutions (last 3 rows) changes from light blue to dark green when the concentration of BG is increased in water. This effect is worse for BP which turns to its acidic form if its concentration is too high. This color change can be explained by the fact that color indicators are weak acids and therefore decrease the pH of the solution when added in water. As a consequence, the color of the solution will change accordingly to the concentration of indicator in solution. The color of BG solutions becomes greener when the concentration is increased because the initial pH of the solution diminishes. Also, the visualization of acidic CO_2 fingers is not possible in a solution of BP 1.000×10^{-3} mol/L, as the initial color of the solution has turned into the acidic form of BP at this concentration. For BG solutions, post-processing procedures generally allow to remove the influence related to the initial color of the solution if only relative changes in pixels intensity are taken into account. Nevertheless, the contrast between the background and CO_2 fingers is lower when the concentration of the dye is small which may cause difficulties in quantitative analysis.

From Fig. 2, it is also clear that the morphology of fingers is different in BP and BG solutions. Although the number of fingers is roughly the same for each experiment, fingers appear much thicker in BP solutions and rapidly connect. In BG solutions, they are on the contrary distinctively separated from each other and are characterized by well contrasted thin bases just below the interface. This characteristic is convenient to draw space–time maps of the dynamics and follow precisely the position of fingers at a fixed depth below the interface in the course of time. A comparison of such space–time maps for BP and BG solutions (concentration of color indicator 1.00×10^{-4} mol/L in both cases) is given in Fig. 3 by plotting, as a function of time, the pixel intensities of the red-channel pictures along the horizontal line at a depth of 2 mm below the interface. In the BG case, the finger dynamics can be easily analyzed near the interface because each finger can be followed individually during its evolution through the bottom of the cell. Statistics on finger merging, splitting, deaths and births can be easily computed at any depth from the maps obtained with BG solutions. For example, we can already see qualitatively that the number of fingers near the interface decreases in the course of time, principally due to merging, as seen in Fig. 2. Following the induction period, fingers appear, start to grow and move laterally to merge with the closest neighbor. Over time, new fingers develop from the boundary layer between existing fingers and follow the same behavior. In the BP case, no relevant information can be obtained from space–time maps where the dynamics of individual fingers becomes rapidly imperceptible. This shows already qualitatively that the "look" of convective fingers is different depending on which color indicator is used. Let us now turn to quantitative analysis of the fingers dynamics for different color indicators in various concentrations.

4.2. Quantitative results

Image processing is performed with the free software ImageMagick to select the area where the dynamics takes place (below the interface) and select the red channel of the RGB

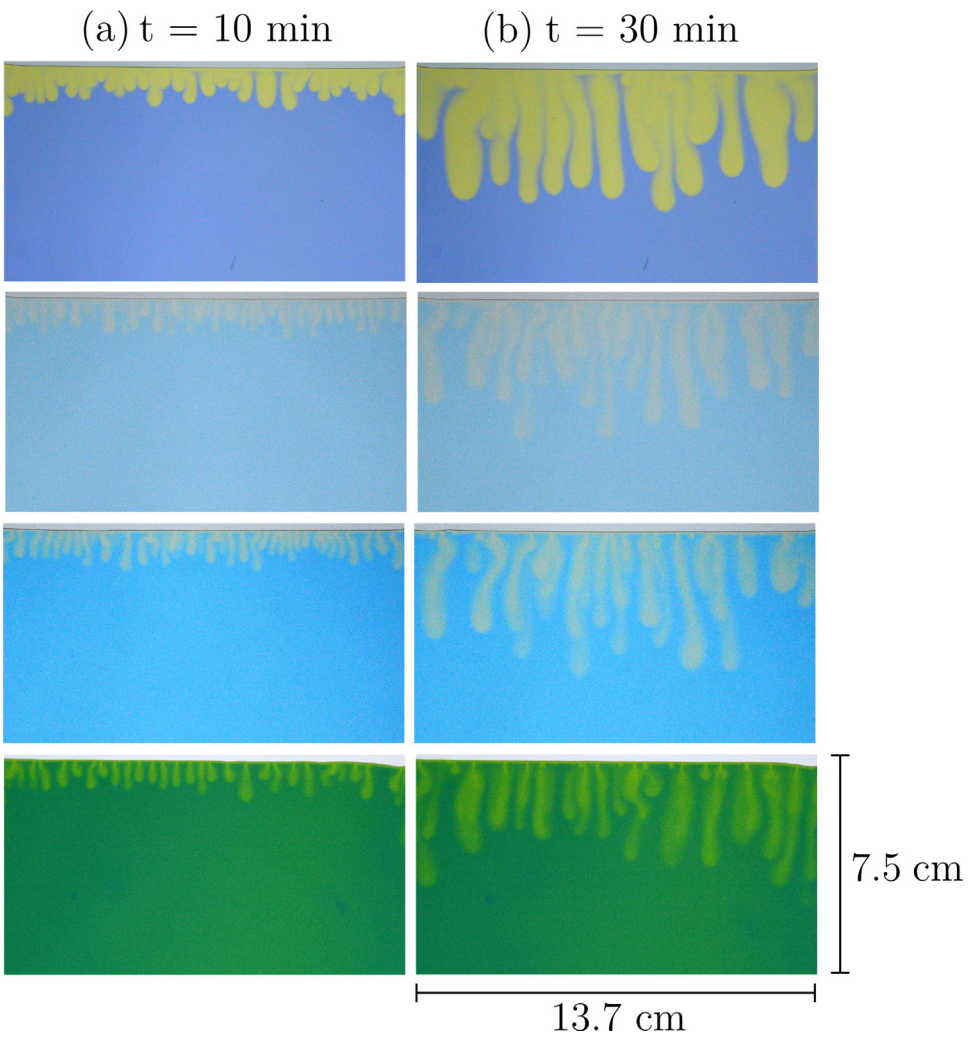

Fig. 2. Development of density driven instability at (a) $t = 10$ min and (b) $t = 30$ min, induced by the dissolution of CO_2 at atmospheric pressure in water containing from top to bottom: bromocresol purple 1.00×10^{-4} mol/L, bromocresol green 5.0×10^{-5} mol/L; 1.00×10^{-4} mol/L; and 1.000×10^{-3} mol/L. The field of view focuses on the lower aqueous phase. Experiments are carried out at room temperature. (For interpretation of the references to color in this figure legend, the reader is referred to the web version of this article.)

pictures, containing the most information about the dynamics and less noise. For each experiment, the selected area has dimensions of 13.7 cm (L_y) × 7.5 cm (L_x). Matlab is then used to subtract the reference image (i.e. before introduction of CO_2 in the cell) from each picture to enhance color changes and reduce the background noise. Each picture gives a two-dimensional matrix c of size $L_y \times L_x$, containing grey values between 0 (black) and 255 (white) and is analyzed to quantify the effect of the indicator on the development of the convective dynamics over time. As the time step between two pictures is 5 s, the time resolution of the following plots is also 5 s.

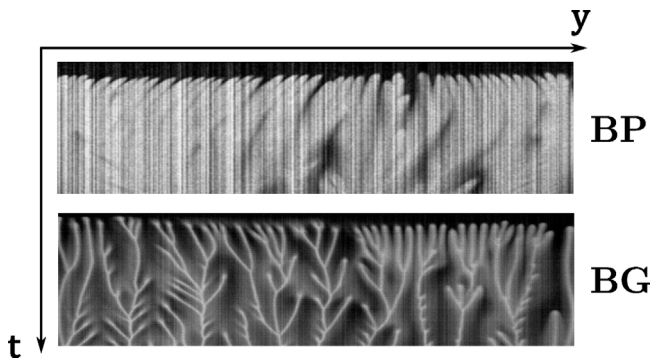

Fig. 3. Space–time maps of the location of fingers at a fixed depth (2 mm below the interface) as a function of time in BP (up) and BG (down) solutions. The concentration of color indicator is 1.00×10^{-4} mol/L in both cases. The field of view is 13.7 cm wide and time is running downwards, $t_{max} = 30$ min.

4.2.1. Evolution of averaged finger length L

In order to measure the averaged finger length L along x (Fig. 4) as a function of time, we first compute the one-dimensional

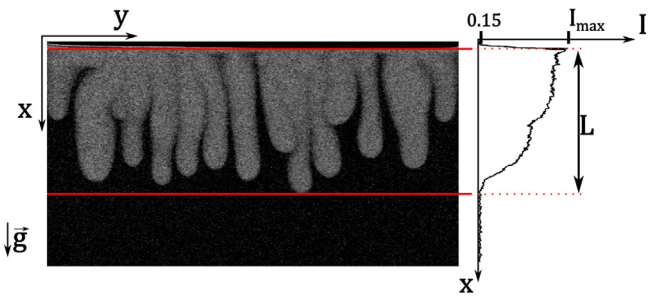

Fig. 4. Processed image of CO_2 fingers in BP solution at $t = 30$ min and corresponding TAP along the x axis. The finger length L is computed as the length of the region where TAP decreases from its maximum value I_{max} (the interface) to 0.15.

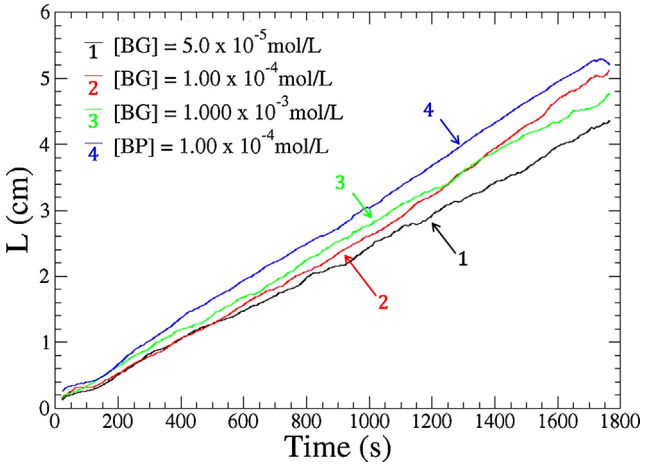

Fig. 5. Temporal evolution of finger length L of CO_2 convective dynamics in BP (1.00×10^{-4} mol/L) and BG (5.0×10^{-5} mol/L; 1.00×10^{-4} mol/L; and 1.000×10^{-3} mol/L) solutions. Each curve represents the average of 5 experiments.

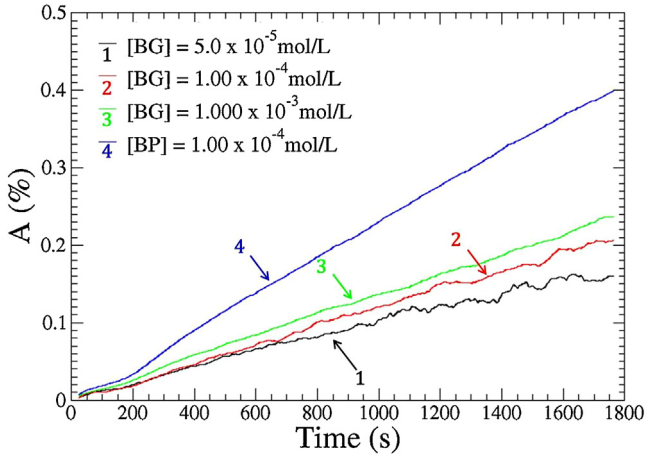

Fig. 6. Temporal evolution of relative area A of the convective pattern in BP (1.00×10^{-4} mol/L) and BG (5.0×10^{-5} mol/L; 1.00×10^{-4} mol/L; and 1.000×10^{-3} mol/L) solutions. Each curve represents the average of 5 experiments.

transverse averaged profile (TAP) at successive times by averaging the 2-D field $c(x, y, t)$ along the transverse coordinate y: $\langle c(x, t)\rangle = \frac{1}{L_y}\int_0^{L_y} c(x, y, t)dy$.

The length L of CO_2 fingers is then computed as the length of the zone in which the TAP $\langle c(x, t)\rangle$ decreases from its maximum value I_{max} (the interface) to 0.15. This lower threshold was arbitrarily defined to follow the tip of the longest finger. Fig. 4 shows a typical experimental post-processed image with the associated TAP and L (at $t = 30$ min). The lengths obtained for five different experiments with the same values of parameters are next averaged and the resulting evolutions are finally smoothed by computing averages over 10 successive points. These averaged lengths L are plotted in Fig. 5 for the four values of parameters of Fig. 2. The averaged standard deviations are 0.2 cm, 0.2 cm, 0.3 cm and 0.4 cm for BG 5.0×10^{-5} mol/L, BG 1.00×10^{-4} mol/L, BG 1.000×10^{-3} mol/L, and BP 1.00×10^{-4} mol/L, respectively.

The temporal evolution of L is qualitatively similar in all solutions (Fig. 5) and is characteristic of the typical development of the buoyancy-driven convective instability detailed above (Fig. 2). When gaseous CO_2 starts to dissolve in the aqueous solution, a thin yellow layer appears below the interface, the length of which grows as a square root of time in the diffusive regime as long as convection does not occur. This diffusive zone is then destabilized after a characteristic time and many small fingers form. As soon as convection sets in, the penetration of dissolved CO_2 in the solution accelerates and L increases almost linearly until the end of the experiment. The characteristic onset time of convection is similar for all experiments and is approximately 100 s (Fig. 5). In BG solutions, the evolution of the finger length is similar for all concentrations except for BG 5.0×10^{-5} mol/L solutions, where fingers seem to grow slower than in other cases after $t = 600$ s. We also observe that L is always larger by a few mm in BP solutions than in all other BG solutions.

4.2.2. Evolution of the relative area A of the convective pattern

The relative area A of the convective pattern is another interesting quantity often computed in CO_2 studies (Kneafsey and Pruess, 2010). This area corresponds to the ratio of the finger area to the total picture area and could a priori be interpreted as an approximate measure of CO_2 uptake. The larger the pattern area, the larger the amount of dissolved CO_2 in solution. For this measure, pictures are binarized to black and white images by applying a threshold, so that fingers appear white on a black background. The area A of the white pattern is calculated at successive times as: $A(t) = \frac{1}{L_x L_y}\int_0^{L_x}\int_0^{L_y} \tilde{c}(x, y, t)dxdy$, where $\tilde{c}(x, y, t)$ is equal to 0 for the black background and to 1 for the white fingers.

The areas averaged over 5 experiments are plotted as a function of time in Fig. 6. The averaged standard deviations are 0.03%, 0.02%, 0.03% and 0.01% for BG 5.0×10^{-5} mol/L, BG 1.00×10^{-4} mol/L, BG 1.000×10^{-3} mol/L, and BP 1.00×10^{-4} mol/L, respectively. The relative area of convective patterns in BP solutions is strikingly larger than in BG solutions. Rapidly after the onset of convection, the evolution of A in BP solutions is much faster and reaches final values twice as large as in experiments with BG solutions. We also observe that A is larger when the concentration of BG in solution increases. The slowest progression is observed for the lowest concentration of BG, which is probably due to the weak contrast between fingers and background, making the edges of the fingers not clearly distinguishable. As a consequence, the binarization of the pictures is more difficult to achieve and results are more sensitive to noise. These observations are in good agreement with the discussion made above In Fig. 2. The buoyancy-driven convective pattern is obviously wider in experiments visualized with BP and this characteristic impacts greatly the measure of A. As the total extent of the convective pattern is dependent on the color indicator in solution, the evolution of A is definitely not a reliable measure to evaluate the CO_2 uptake if the pattern is visualized with this technique.

4.3. Interpretation of experimental results

The explanation for the results obtained may be related to the visualization of different iso-pH zones by color indicators. If we consider the pH field within a single finger, the pH is not homogeneous inside the finger but evolves along iso-pH curves with decreasing pH values from finger edges to the center where the lowest pH values are found, corresponding to the largest concentrations of dissolved CO_2. Color indicators highlight areas where the pH decreases below their specific transition range. The visualization of a finger by a given color indicator will be consequently limited to the iso-pH curve corresponding to the lower value of its transition range and will not be the same than with other color indicators having different transition ranges.

In order to confirm this hypothesis, we visualized CO_2 convective dissolution in a solution of water containing a universal color indicator[1] which is sensitive to pH variations between 4 and 10.

[1] Liquid mixture of pH sensitive dyes which includes phenolphthalein, bromothymol blue, methyl red, and thymol.

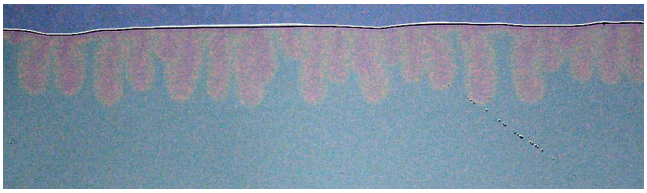

Fig. 7. Convective pattern induced by CO_2 dissolution in water containing a universal color indicator. This indicator is sensitive to pH variations in a range from 4 to 10 and is able to highlight different iso-pH zones inside the fingers. (For interpretation of the references to color in this figure legend, the reader is referred to the web version of this article.)

As this indicator gradually displays a different color for each pH value, it can reveal more than two zones of the pH field characterizing the solution. An example of the convective pattern observed at ~8 min after beginning of experiment is shown in Fig. 7. Even if the concentration of the universal color indicator is higher than the recommended values (3 droplets of liquid indicator per 5 ml of water), the color intensity of the initial solution is very weak and the fingering pattern is barely visible with the naked eye. A strong contrast enhancement is necessary to distinguish the different colored areas and the original colors are slightly altered. Nevertheless, we can observe on Fig. 7 that each finger is composed of 2 different colors: pink and yellow, corresponding originally to red and orange. Following the color chart of the universal indicator, red and orange correspond approximately to pH 4 and 5 respectively. Most of the pattern is red and is similar to the area visualized by BG. A secondary orange area surrounding the red zone connects some fingers between them, giving a total area which seems to correspond to the pattern visualized by BP.

These results explain why the pattern visualized by BP has a little larger length than BG and a larger area. Indeed, as BP turns yellow as soon as the pH decreases below 5.2, the extent of acidic yellow fingers in BP solutions will be wider than with BG which is only able to detect areas where the pH has decreased below 3.8 (red areas showed by the universal color indicator on Fig. 7). Areas where the pH has decreased but remains above 3.8 (orange areas on Fig. 7) are therefore not visualized by BG. The visualization of the convective pattern is thus clearly affected by the characteristics of the color indicator selected to perform the study.

5. Effect of color indicator in alkaline conditions

These results suggest that some part of the dynamics may not be visualized if the fingers have a larger extent than the visualized iso-pH curve equivalent to the color transition value of the chosen indicator. To investigate this assumption, additional experiments have been performed with the help of a Schlieren system (Settles, 2001). A Z-type Schlieren system is used here and is shown schematically in Fig. 8. It is composed of two 20 cm diameter parabolic mirrors with 1 m focal lengths, a LED as a white light source, a knife edge and a CCD monochromatic camera. This configuration provides a visualization of the dynamics by tracking gradients of refractive index related to density gradients, and allows to follow the dynamics in real time without interfering with it.

As convection due to CO_2 dissolution is difficult to visualize in water by Schlieren techniques (density gradients are small and need a very sensitive set up to be detected), solutions of NaOH are used to study CO_2 buoyancy-driven convection. With NaOH in solution, chemical reactions between the base and the dissolved CO_2 take place, generating a product much denser than the reactants (Thomas et al., 2014). The development of the fingering instability in NaOH solutions is consequently faster and the resulting density gradients are larger than in water, generating larger refractive

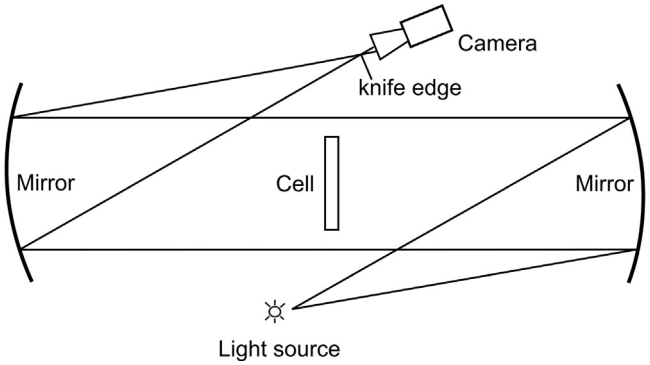

Fig. 8. Schematic of the Z-type Schlieren system used to visualize buoyancy-driven convection of CO_2 in NaOH solutions. Our set-up is composed of two 20 cm diameter mirrors with 1 m focal lengths. The Hele-Shaw cell is placed between the two mirrors and a CCD monochromatic camera records the dynamics at successive times.

index gradients and the convective dynamics is therefore easier to visualize.

The goal of this section is double: first, we compare qualitatively the dynamics recorded in NaOH solutions containing a color indicator by the direct visualization of color changes and by the Schlieren system in order to check if visualizations of the convective patterns are the same. For this purpose, we temporarily added a color camera and a beamsplitter to the Z-type Schlieren system. This configuration allows to simultaneously visualize the convection pattern with the Schlieren set-up and to take pictures of color changes. Secondly, the development of CO_2 fingers growing in NaOH solutions without color indicator is compared with the case where NaOH solutions contain different color indicators in order to determine if the presence of a color indicator affects the development of the dynamics.

The liquid phases considered are either aqueous solutions of NaOH only or NaOH solutions containing 3 different color indicators (all color indicators are studied separately): bromocresol green (BG, transition range: 5.4–3.8), bromocresol purple (BP, transition range: 6.8–5.2) and phenol red (PR, transition range: 8.4–6.6). The Hele-Shaw cell is placed in the Schlieren system and the same experimental procedure is applied as described in Section 2. An example of pattern imaged with the Schlieren set-up is given in Fig. 9. The development of the fingering instability is qualitatively similar to that in water containing BG or BP but is faster (Thomas et al., 2014). First, the onset time of convection in solutions of NaOH 2.000×10^{-2} mol/L is approximately 30 s, which is more than 3 times smaller than the onset time observed in water containing BG or BP (~100 s). Then, the rate at which fingers grow in time is larger in NaOH solutions than in water.

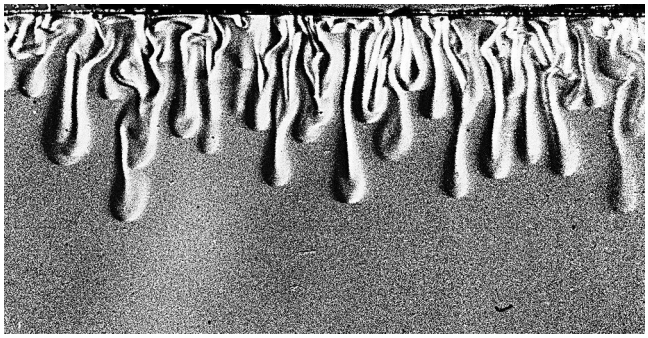

Fig. 9. Schlieren view of the CO_2 convective dynamics at $t = 10$ min in a solution of NaOH 2.000×10^{-2} mol/L. The field of view is 11.7 cm wide.

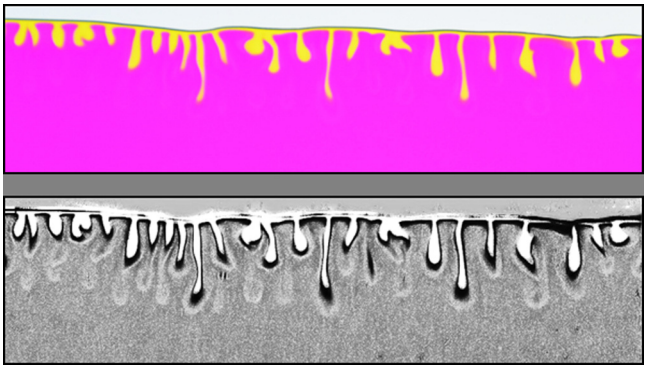

Fig. 10. Comparison of CO_2 convective dynamics at $t = 300$ s in a solution of NaOH (1.000×10^{-2} mol/L) containing phenol red (5.0×10^{-4} mol/L) by direct visualization of color changes (up) and by Schlieren visualization (down). (For interpretation of the references to color in this figure legend, the reader is referred to the web version of this article.)

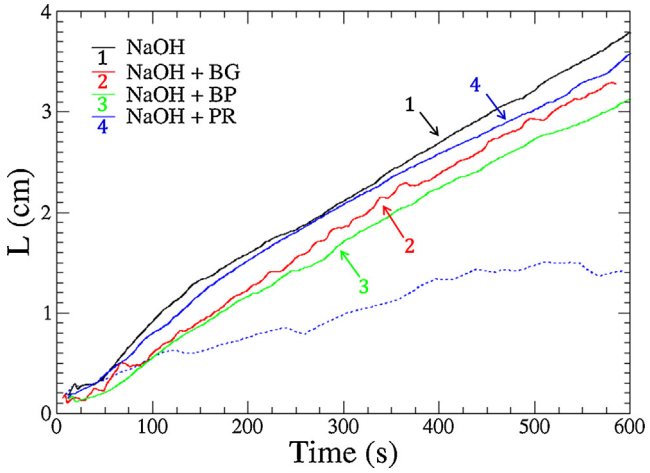

Fig. 11. Full curves: temporal evolution of finger length L, computed from the Schlieren view of CO_2 convective dynamics in NaOH solutions containing a color indicator or not. Dashed curve: fingers growth visualized directly by color changes of PR. The concentration of NaOH and color indicators are 2.000×10^{-2} mol/L and 2.50×10^{-3} mol/L, respectively. Each curve represents the average of 5 experiments. (For interpretation of the references to color in the text, the reader is referred to the web version of this article.)

The decrease of pH due to CO_2 dissolution in the aqueous solution is here difficult to predict because chemical reactions between NaOH and dissolved CO_2 are complex. Indeed, the amount of dissolved CO_2 and the rate of dissolution are affected by those reactions, it is therefore impossible to determine the concentration of dissolved CO_2 in solution. However, the initial pH of the basic solution is ~ 12 and a clear change of color following introduction of gaseous CO_2 in the cell is observed in solutions containing PR, which means that the pH of the aqueous solution can locally decrease below 6.6. As the pH decrease in NaOH solutions is here beyond the transition range of BG and BP, those indicators are unable to highlight the dynamics showed by the Schlieren system and no change of color is observed in solutions containing BG and BP during these experiments in alkaline conditions.

5.1. Comparison of visualization techniques

Phenol Red appears thus to be able to detect CO_2 dissolution (basic form: pink - acid form: yellow) in NaOH solutions. We first visualized qualitatively the dissolution of gaseous CO_2 in a solution of NaOH 1.000×10^{-2} mol/L containing PR 5.0×10^{-4} mol/L. We observed that the development of the convective dynamics obtained with the Schlieren system and the direct visualization of color changes are similar in early stages of experiments but differ after a few minutes. Indeed, soon after the injection of CO_2 in the cell, a bright yellow line appears below the interface in the presence of PR, exactly like in experiments with water containing BG and BP. We can observe a sharp color contrast between the two forms of phenol red, indicating that the acidic form of the color indicator fully dominates and that the pH locally decreases below 6.6. But soon after the onset of convection, differences between the Schlieren visualization and color changes appear, as shown in Fig. 10 which compares the two visualizations of the same dynamics in the solution at $t = 300$ s. Black and white areas on the Schlieren image also correspond to areas where the color of the solution has changed because this technique is also sensitive to color changes in the solution. Nevertheless, the Schlieren visualization also shows surrounding lighter gray areas, distinct from the background, meaning that the density-driven convective area is more extended than the zone where the color of PR changes. This indicates that, even if the color transition of the pH indicator is observed, PR is not appropriate to detect the total extent of the convection zone in these conditions. Furthermore, we see that the pH is inhomogeneous inside a finger and cannot be easily related to density gradients. This figure is clearly an example where pH and density gradients do not give the same information on the convective pattern. Generally, optical systems detect refractive index gradients that can, in some cases, be related to density and concentration fields (Wylock et al., 2011; Hargather and Settles, 2012; Settles, 2001). Although the relation between refractive index, density and concentration gradients remains difficult to establish in the case of CO_2 convective dissolution, the refractive index is the closest measurable quantity to density, which is the driving force of the convective instability. Schlieren or interferometric techniques are therefore more adapted to visualize density-driven convection.

In order to obtain a higher contrast between the convective pattern and the background, and measure the length of the fingers, the concentration of NaOH was increased to 2.000×10^{-2} mol/L. With this concentration, the dynamics is affected by chemical reactions. The concentration of color indicator was thus also increased to the solubility limit 2.50×10^{-3} mol/L.

5.2. Evolution of averaged finger length L in NaOH solutions

Post-processing of Schlieren images like shown in Fig. 9 is done following the same guidelines as detailed in Section 4 and temporal evolutions of finger lengths L obtained for five experiments are averaged. As mentioned in the previous section, the Schlieren technique is also sensitive to color changes appearing in solution, filtering the light rays passing through the cell. The pink-yellow transition occurring in PR solutions is therefore clearly visible on Schlieren pictures (as seen on Fig. 10). In addition, the averaged finger length L is also computed from color changes of PR by binarizing the pictures with a threshold high enough to keep these color changes only. Fig. 11 shows the evolution of these averaged lengths in solutions of NaOH 2.000×10^{-2} mol/L containing a color indicator or not. Full curves focus exclusively on the Schlieren visualization of the dynamics and the dashed curve represents the fingers growth visualized by color changes of PR. As fingers were not visualized directly in solutions containing BG, BP or NaOH only, the corresponding dashed curves are not plotted ($L = 0\ \forall t$). The averaged standard deviations are 0.1 cm for NaOH only and 0.2 cm for the other curves.

For the Schlieren visualization (full curves), the evolution of L is similar in all experiments, except for solutions containing NaOH only and PR where fingers grow faster during the first 100 s after

the onset of convection. It then decelerates to a linear evolution like in solutions containing BG and BP, and fingers finally reach similar grow rates in all solutions during the last 200 s of experiment. This shows that the presence or not of an indicator in solution does not really affect the development of the buoyancy-driven fingering. This may be due to the fact that the chemical reactions involved by the presence of NaOH in solution control the dynamics, masking the impact of the indicator in the solution. But if we compare the growth of fingers in NaOH solutions containing PR, visualized either by the Schlieren system or by color changes of PR (blue full and dashed curves), we can see that the evolution of L based on color changes only is strongly inaccurate. As expected from Fig. 10, fingers directly visualized by color changes of PR are significantly smaller than those observed with the Schlieren system as a part of their area is missed by the pH indicator.

6. Conclusion

This work has focused on analyzing experimentally the impact of the use of color indicators on the visualization of fingering instabilities in aqueous solutions. In the particular case of CO_2 dissolution, several species (CO_2, HCO_3^-, CO_3^{2-}) are present in the solution depending on its initial composition and the amount of dissolved CO_2 in the system. When convective instabilities develop due to the dissolution in water of CO_2, a pH gradient will be formed around the fingers, with a central acidic core where the concentration of CO_2 reaches a maximum. Considering the range where the color of the pH indicator changes and the pH field originated by the dissolution of CO_2 in water, we showed that the shape and hence the characteristics of the convective pattern visualized strongly depend on the color indicator selected to perform the study. When CO_2 was dissolved in water containing bromocresol purple, the area detected was larger than in bromocresol green solutions. The evaluation of the area A of the fingers was much more sensitive than that of the finger length L to the use of different indicators, probably because of the geometry of the fingers. To confirm the effect of the indicator, the CO_2 dissolution pattern in a solution of NaOH was studied both by a Schlieren technique tracking gradients of index of refraction and with colored images obtained with an indicator (phenol red). In this case, even if the presence of a color indicator in the solution did not seem to impact the development of the convective dynamics, Schlieren visualization imaged longer and thicker fingers than those obtained with phenol red. This shows that color indicators should be used with caution in experimental studies of convective processes as the patterns they detect reflect only the pH field to which the indicator is sensitive. Color indicators hence do not necessarily show the whole extent of the convective dynamics, giving rise to possible inaccurate quantitative characterization of the patterns. Optical imaging techniques tracking gradients of refractive index like Schlieren or interferometry should therefore be favored to visualize buoyancy-driven convection in Hele-Shaw cells.

Acknowledgements

We thank F. Haudin, V. Loodts, L. Rongy, D.M. Escala and P. Bunton for fruitful discussions. C.T. and A.D. (ULB) acknowledge financial support from the FRS-FNRS FORECAST project.

References

Almarcha, C., Trevelyan, P.M.J., Riolfo, L.A., Zalts, A., El Hasi, C., D'Onofrio, A., De Wit, A., 2010. Active role of a color indicator in buoyancy-driven instabilities of chemical fronts. J. Phys. Chem. Lett. 1, 752.

Arendt, B., Dittmar, D., Eggers, R., 2004. Interaction of interfacial convection and mass transfer effects in the system CO_2-water. Int. J. Heat Mass Transf. 47, 3649.

Backhaus, S., Turitsyn, K., Ecke, R.E., 2011. Convective instability and mass transport of diffusion layers in a Hele-Shaw geometry. Phys. Rev. Lett. 106, 104501.

Blair, L.M., Quinn, J.A., 1968. Measurement of small density differences: solubility of slightly soluble gases. Rev. Sci. Instrum. 39, 75.

Budroni, M.A., Riolfo, L.A., Lemaigre, L., Rossi, F., Rustici, M., De Wit, A., 2014. Chemical control of hydrodynamic instabilities in partially miscible two-layer systems. J. Phys. Chem. Lett. 5, 875.

Cardoso, S.S.S., Andres, J.T.H., 2014. Geochemistry of silicate-rich rocks can curtail spreading of carbon dioxide in subsurface aquifers. Nat. Commun. 5, 5743.

Elenius, M.T., Johannsen, K., 2012. On the time scales of nonlinear instability in miscible displacement porous media flow. Comput. Geosci. 16, 901.

Ennis-King, J., Paterson, L., 2005. Role of convective mixing in the long-term storage of carbon dioxide in deep saline formations. SPE J. 10, 349.

Faisal, T.F., Chevalier, S., Sassi, M., 2013. Experimental and numerical studies of density driven natural convection in saturated porous media with application to CO_2 geological storage. Energy Procedia 37, 5323.

Firoozabadi, A., Cheng, P., 2010. Prospects for subsurface CO_2 sequestration. AIChE J. 56, 1398.

Hargather, M.J., Settles, G.S., 2012. A comparison of three quantitative Schlieren techniques. Opt. Lasers Eng. 50, 8.

Hassanzadeh, H., Pooladi-Darvish, M., Keith, D.W., 2005. Modelling of convective mixing in CO_2 storage. J. Can. Pet. Technol. 44, 43.

Hassanzadeh, H., Pooladi-Darvish, M., Keith, D.W., 2006. Stability of a fluid in a horizontal saturated porous layer: effect of non-linear concentration profile, initial, and boundary conditions. Transp. Porous Med. 65, 193.

Haynes, W.M., 2014. Handbook of Chemistry and Physics, 95th Edition. CRC Press.

Hidalgo, J.J., Fe, J., Cueto-Felgueroso, L., Juanes, R., 2012. Scaling of convective mixing in porous media. Phys. Rev. Lett. 109, 264503.

Khosrokhavar, R., Elsinga, G., Farajzadeh, R., Bruining, H., 2014. Visualization and investigation of natural convection flow of CO_2 in aqueous and oleic systems. J. Pet. Sci. Eng. 122, 230.

Kilpatrick, A., Rochelle, C., Noy, D., 2011. Experimental visualisation and modelling of the formation and migration of density plumes during CO_2 storage. In: Flows and mechanics in natural porous media from pore to field scale. Pore2Field.

Kim, M.C., 2014. Miscible gravitational instability of initially stable horizontal interface in a porous medium: Non-monotonic density profiles. Phys. Fluids 26, 114102.

Kirk, K., Vosper, H., Rochelle, C., Noy, D., Chadwick, A., 2014. Development of density plumes of dissolved CO_2: comparing experimental observations with numerical simulations. Geophys. Res. Abstr. 16, EGU2014-10001-2.

Kneafsey, T.J., Pruess, K., 2010. Laboratory flow experiments for visualizing carbon dioxide-induced, density-driven brine convection. Transp. Porous Media 82, 123.

Kneafsey, T.J., Pruess, K., 2011. Laboratory experiments and numerical simulation studies of convectively enhanced carbon dioxide dissolution. Energy Procedia 4, 5114.

Kuster, S., Riolfo, L.A., Zalts, A., El Hasi, C., Almarcha, C., Trevelyan, P.M.J., De Wit, A., D'Onofrio, A., 2011. Differential diffusion effects on buoyancy-driven instabilities of acid-base fronts: the case of a color indicator. Phys. Chem. Chem. Phys. 13, 17295.

MacMinn, C.W., Juanes, R., 2013. Buoyant currents arrested by convective dissolution. Geophys. Res. Lett. 40, 2017.

Metz, B., Davidson, O., de Conninck, H.C., Loos, M., Meyer, L.A., 2005. IPCC special report on carbon dioxide capture and storage. Prepared by working group III of the Intergovernmental Panel on Climate Change. Cambridge University Press.

Mojtaba, S., Behzad, R., Rasoul, N.M., Mohammad, R., 2014. Experimental study of density-driven convection effects on CO_2 dissolution rate in formation water for geological storage. J. Nat. Gas Sci. Eng. 21, 600.

Neufeld, J.A., Hesse, M.A., Riaz, A., Hallworth, M.A., Tchelepi, H.A., Huppert, H.E., 2010. Convective dissolution of carbon dioxide in saline aquifers. Geophys. Res. Lett. 37, L22404.

Okhotsimskii, A., Hozawa, M., 1998. Schlieren visualization of natural convection in binary gas-liquid systems. Chem. Eng. Sci. 53, 2547.

Outeda, R., El Hasi, C., D'Onofrio, A., Zalts, A., 2014. Experimental study of linear and nonlinear regimes of density-driven instabilities induced by CO_2 dissolution in water. Chaos 24, 013135.

Pau, G.S.H., Bell, J.B., Pruess, K., Almgren, A.S., Lijewski, M.J., Zhang, K., 2010. High-resolution simulation and characterization of density-driven flow in CO_2 storage in saline aquifers. Adv. Water Resour. 33, 443.

Riaz, A., Hesse, M., Tchelepi, H.A., Orr Jr., F.M., 2006. Onset of convection in a gravitationally unstable, diffusive boundary layer in porous media. J. Fluid Mech. 548, 87.

Settles, G.S., 2001. Schlieren and shadowgraph techniques: visualizing phenomena in transparent media. Springer-Verlag.

Slim, A.C., Bandi, M.M., Miller, J.C., Mahadevan, L., 2013. Dissolution-driven convection in a Hele-Shaw cell. Phys. Fluids 25, 024101.

Song, Y., Chen, B., Nishio, M., Akai, M., 2005. The study on density change of carbon dioxide seawater solution at high pressure and low temperature. Energy 30, 2298.

Thomas, C., Loodts, V., Rongy, L., De Wit, A., 2014. Control of convective dissolution by chemical reactions: general classification and application to CO_2 dissolution in reactive aqueous solutions. Phys. Rev. Lett. 113, 114501.

Tsai, P.A., Riesing, K., Stone, H.A., 2013. Density-driven convection enhanced by an inclined boundary: implications for geological CO_2 storage. Phys. Rev. E 87, 011003.

Wylock, C., Dehaeck, S., Cartage, T., Colinet, P., Haut, B., 2011. Experimental study of gas-liquid mass transfer coupled with chemical reactions by digital holographic interferometry. Chem. Eng. Sci. 66, 3400.

Wylock, C., Dehaeck, S., Alonso Quintans, D., Colinet, P., Haut, B., 2013. CO_2 absorption in aqueous solutions of N-(2-hydroxyethyl)piperazine: experimental characterization using interferometry and modeling. Chem. Eng. Sci. 100, 249.

Wylock, C., Rednikov, A., Haut, B., Colinet, P., 2014. Nonmonotonic Rayleigh-Taylor instabilities driven by gas-liquid CO_2 chemisorption. J. Phys. Chem. B 118, 11323.

Yang, C., Gu, Y., 2006. Accelerated mass transfer of CO_2 in reservoir brine due to density-driven natural convection at high pressures and elevated temperatures. Ind. Eng. Chem. Res. 45, 2430.